Journal of Applied Electrochemistry **30**: 419–427, 2000.

Texture prediction of Bi_2Te_3 electroplated layers using Hartman's theory of crystal growth

H. CHAOUNI, J. BESSIÈRES, A. MODARESSI and J.J. HEIZMANN
LETAM URA2090 CNRS/GMPC/ISGMP, Ile du Saulcy, 57045 METZ Cedex 1, France

Received 29 October 1996; accepted in revised form 13 April 1999

Key words: bismuth telluride, crystal growth, texture

Abstract

An experimental study of electroplated thin films of bismuth telluride, $R\bar{3}m$ crystal structure, shows that fibre textures are observed during the growth of the layers. Several orientations $\langle 00.1\rangle$, $\langle 10.10\rangle$, $\langle 11.0\rangle$, $\langle 10.4\rangle$, $\langle 10.8\rangle$, $\langle 01.5\rangle$ and $\langle 10.0\rangle$ are developed during the deposition process, then reach a final orientation. Hartman's theory of crystal growth based on the periodic bond chain (PBC) in a crystal lattice is usually applied. This explains the equilibrium shape of a crystal defined by F faces and the faces observed during the growth (S and K faces). It also successfully predicts the orientations observed in bismuth telluride from the beginning to the end of the layer deposition. The theory may also be applied to other deposition processes.

1. Introduction

Among the large variety of deposition methods producing thin layers, electrodeposition is used to obtain thicknesses ranging between a micrometre to several tens of micrometres, with high deposition speeds. During deposition, important steps occur, namely, nucleation, coalescence of nuclei and growth of the nuclei. This crystalline growth leads to a coating in which crystallites are more or less oriented with respect to the substrate. These preferential orientations give deposits with different physical, chemical and mechanical properties.

Texture, or crystallite orientation, development during the growth of the deposit depends on nucleation and growth processes [1], but some work attempts to link observed textures to nucleation and growth conditions, which vary with experimental parameters such as vapour pressure, temperature and substrate surface state. For electrolytic processes some specific parameters, such as current density, voltage, composition and concentration of electrolyte baths, can also affect the texture [2].

To contribute to a better understanding of electrodeposition mechanisms, we have chosen to study deposits of the bismuth telluride ($Bi_{2-x}Te_{3+x}$), which has important anisotropic properties [3] due to the great ratio c/a (6.92) of the crystal unit cell, the thermoelectric efficiency of Bi_2Te_3 depends on the crystallographic orientation of grains and the homogeneity of the deposit. Any dispersion of the orientation decreases the thermoelectric efficiency. This motivates the study of the texture of this material. According to Hartman's theory of crystal growth [4–6], the crytallographic orientations of the deposited layers may be explained.

2. Crystallographic texture

2.1 *What is the crystallographic texture?*

The crystallographic texture describes the orientations of the different grains of the material according to reference axes $\{Oxyz\}$ fixed on the sample which is, in the present case, the substrate. These orientations are usually obtained by X-ray diffraction on the lattice planes, $(h\,k\,l)$, of the grains [7, 8].

The diffracted intensity is proportional to the volume fraction of the grains having the orientation which fulfils Bragg's law. To detect all the grains having different orientations the sample must have two rotations: a tilt ψ from the sample normal direction and an azimuthal rotation φ. When the sample is tilted, with an angle ψ, all the lattice planes $(h\,k\,l)$ of grains whose normals $[h\,k\,l]^*$ lie on a ψ aperture cone can be detected during the azimuthal rotation (Figure 1). Scanning $0° < \psi < 80°$ and $0° < \varphi < 360°$, with $\Delta\psi = 2.5°$ and $\Delta\varphi = 5°$, is used in our case to detect all orientations.

The diffracted intensity at position (ψ, φ), which also represents the density of the normal $[h\,k\,l]^*$ at this given position, is plotted on a stereographic projection, in the plane of the sample (Figure 2). Points having the same intensity are joined together and give level lines. This stereographic projection is the pole figure $h\,k\,l$. The different levels are given in a normalized scale where the level 1 represents isotropy (randomly oriented sample).

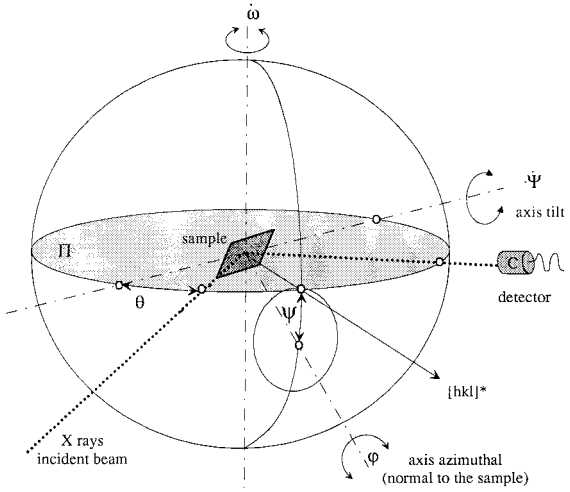

Fig. 1. Illustration of the Schulz goniometric arrangement. Π is the incidence plane defined by the incident beam and the diffracted beam collected by the detector. For a given ψ tilting angle during the φ rotation, the detected lattice planes have their normals $[h\,k\,l]^*$ on a cone of aperture ψ tangent to the incidence plane.

To study the texture of Bi_2Te_3, deposits were prepared under different electrodeposition conditions. A texture goniometer, configured to record simultaneously several pole figures and their background, was used. Intensity corrections were done according to the thicknesses of the layers [9]. X-rays diffracted by the sample were detected by a curved position-sensitive detector (INEL CPS 120) having a 120° angular aperture.

2.2. *Structure of bismuth telluride*

Bismuth telluride has a rhombohedral structure (space group $R\bar{3}m$), whose unit cell parameters are: $\alpha = 24°.08'$ and $a_r = 10.47$ Å. The structure can equally be considered as a hexagonal one with parameters: $a_H = 4.3835$ Å and $c_H = 30.360$ Å (Figure 3) [13]. Through the c_H axis or $[1\,1\,1]_R$ direction, the structure can be seen as a stacking of bismuth or tellurium atomic planes, these planes being arranged in three quintets along the period of the c_H axis: $Te^{(2)}$–Bi–$Te^{(1)}$–Bi–$Te^{(2)}$ indexes (1) and (2) are used to distinguish coordination of tellurium atoms. $Te^{(1)}$ has six bismuth atoms as first neighbours,

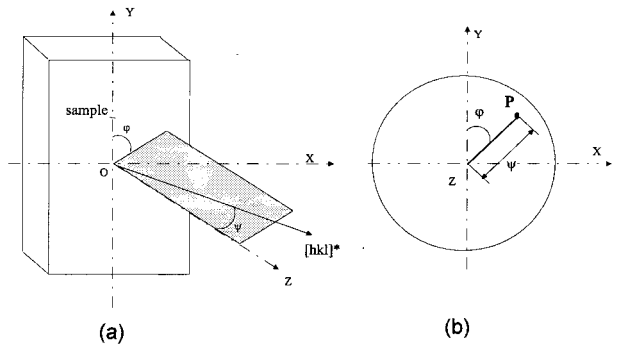

Fig. 2. (a) A normal $[h\,k\,l]^*$ is located by angles (ψ, φ) with respect to the sample; (b) stereographic projection P of this normal on the plane (xOy) of the sample.

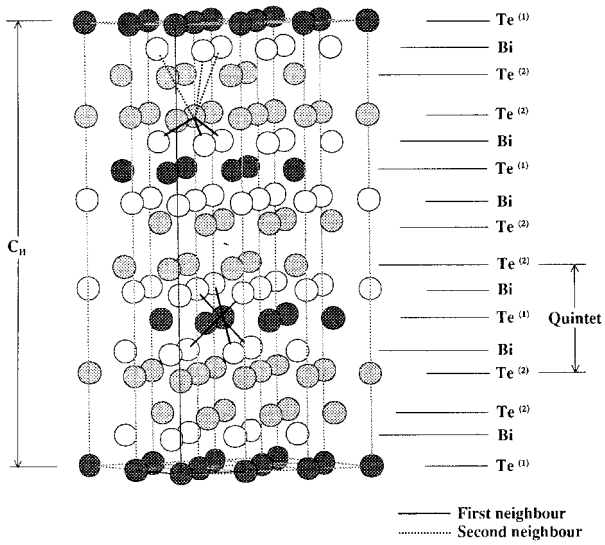

Fig. 3. Structure of Bi_2Te_3 and bonds between atoms of Bi and Te.

while $Te^{(2)}$ has three bismuth atoms as first neighbours [14].

2.3. *Preparation of the samples*

Bismuth telluride films of uniform thicknesses were prepared by electrodeposition from a solution containing Bi^{3+} and $HTeO_2^+$ according to the following reaction:

$$3\,HTeO_2^+ + 2\,Bi^{3+} + 18\,e^- + 9H^+ \longrightarrow Bi_2Te_3 + 6\,H_2O$$

The electrolytes were prepared, at a constant temperature of 25 °C, with deionized water. To ensure the stability and the solubility of the bismuth(III) solutions, the selected solvent was 1 M aqueous HNO_3. The Bi^{3+} solution were obtained by dissolution of $Bi(NO_3)_3 \cdot 5\,H_2O$ (analytical grade). The Te^{4+} solutions were prepared from the reaction of nitric acid on high purity elemental tellurium. Under these acidic conditions, tellurium was in the form of $HTeO_2^+$ (telluryl ion).

The Bi^{3+} and $HTeO_2^+$ electrolyte mixture were obtained from the above solutions, and the $Bi^{3+}/HTeO_2^+$ ratios were varied to predetermined values.

The composition of products removed from the support was analysed using several techniques: electron probe microanalysis (CAMECA SX 50) calibrated with tellurium (purity 99.9%) and bismuth (purity 99.9%) standards [10] or a volumetric method [11] or X-ray diffraction [12]. Layers of Bi_2Te_3 of different thicknesses from 1 μm to 50 μm were prepared.

3. Experimental results

3.1. *Variations of the texture with the thickness*

Bi_2Te_3 layers, ranged between 0.3 and 20 μm, were deposited at a 45 A m^{-2} current density on stainless steel which was initially polished with carborundum paper

and with diamond paste (1 μm size) and finally electropolished. The θ–2θ diffractogram presented in Figure 4 shows only Bi_2Te_3 and/or $Bi_{2+x}Te_{3-x}$ which have a similar (trigonal $R\bar{3}m$) structure. To determine orientations of the coating, three pole figures of the lattices planes $(11.0)_H$, $(01.5)_H$ and $(10.10)_H$, given in the equivalent hexagonal unit cell, were chosen because they have relatively high intensities without interference from diffraction lines of the steel.

All pole figures present concentric rings characteristic of fibre textures. Figure 5 shows the three pole figures $(11.0)_H$, $(01.5)_H$ and $(10.10)_H$ of the 20 μm thick layer. These pole figures correspond to a fibre texture where the $[11.0]^*_H$ axis is perpendicular to the surface of the sample. The theoretical ring location corresponding to the observed lattices planes is shown in Figure 5(d) and agrees with the experimental observations.

In other words, the main part of grains, which have grown on the layer, have a lattice plane (11.0), which is parallel to the surface of the steel. The $\vec{c}$ axis of the structure, belonging to the (11.0) plane, is parallel to the surface of the steel, and is randomly distributed in the surface because continuous rings are observed on the pole figure.

The 5 μm thick sample presents a fibre $[10.10]^*$ perpendicular to the surface of the sample. The 1 μm thick sample presents $[10.8]^*$ fibre texture.

Pole figures of 0.3 μm thick sample have not revealed anything because the thickness of the deposit is too thin and because there is too much orientations (Figure 6(a) and (e)) to obtain enough X-ray diffraction intensity, which is necessary to detect the orientations.

These experiments, where thicknesses differ, show different orientations according to the thickness of the layer. For the thicker layer, the deposit orients to a fibre texture $[11.0]^*_H$. This orientation is also seen on the 20 μm thick layer of Bi_2Te_3 deposited on aluminium (Figure 6).

3.2. *Texture evolution with the substratum*

Deposits 5 μm and 20 μm thick on aluminium and steel substratums, prepared with a current density of 45 A m^{-2}, were studied. To avoid overlap with the diffraction line of aluminium we chose to measure pole figures $(01.5)_H$, $(11.0)_H$ and $(20.5)_H$.

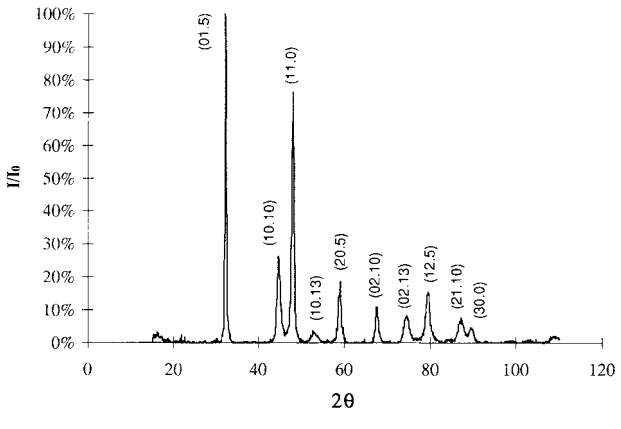

Fig. 4. Diffractogramm of Bi_2Te_3 20 μm thick.

The 5 μm thick layer on aluminium shows a $[01.5]^*_H$ fibre axis perpendicular to the surface of the sample (Figure 7). Pole figures for the 20 μm thick layer on aluminium show that the fibre axis $[11.0]^*_H$ is perpendicular to the surface of the sample (Figure 8). For the 5 μm thick layer deposited on steel, the orientation of Bi_2Te_3 is different, as it was previously seen.

It appears that, for thin layers, the substrate has an influence on the orientation of deposits but when the thickness of the deposit increases and reaches a sufficient thickness, which is less than 20 μm, the substrate does not affect the orientation, which becomes a $[11.0]^*_H$ fibre (Figure 6(d) and (h)).

3.3. *Texture evolution with current density*

Deposits were obtained at two current densities 45 and 225 A m^{-2}. Their thicknesses were 5.3 μm. The pole figure analysis of these samples shows that current density has an influence on the orientation of the deposits. The layers deposited on a steel substrate (45 A m^{-2}) have a fibre $[10.10]^*_H$, while they have two fibres, $[00.1]^*_H$ and $[10.4]^*_H$, when 225 A m^{-2} is used. Similarly, for layers deposited on aluminium, the layers deposited at 45 A m^{-2} leads to a fibre $[01.5]^*$, while the layer deposited at 225 A m^{-2} gives a fibre $[01.8]^*$.

3.4. *Stoichiometry in $Bi_{(2-x)}Te_{(3+x)}$ deposits*

The conditions of synthesis (Bi/Te ratio in the electrolytic bath), and therefore the stoichiometry of the deposits of bismuth telluride, seems to play an essential role on the electrical properties of the compound. This is why we studied the texture of layers whose Bi/Te ratio changed from 0.33 to 0.45. Different orientations were observed: $\langle 11.0\rangle^*$, $\langle 10.10\rangle^*$, $\langle 10.8\rangle^*$, $\langle 01.5\rangle^*$ and $\langle 00.1\rangle^*$. It can therefore be concluded that texture is linked to the stoichiometry of the compound. The conductivity being highest in the lattice plane $(00.1)_H$ [11], the electroformed layer offers theoretically the best electrical properties, when $(00.1)_H$ lattice planes are perpendicular to the surface of the substrate; thus all $\langle h\,k.0\rangle^*$ fibre orientations would be favourable. It appears that the compound which is the closest to the stoichiometry, will be the most powered.

3.5. *Summary of the texture observations*

The main texture observations are as follows: (i) fibres textures are always observed, and (ii) according to substrate, current density, thickness and stoichiometry of the layer, different fibres $\langle 00.1\rangle^*$, $\langle 10.10\rangle^*$, $\langle 11.0\rangle^*$, $\langle 10.4\rangle^*$, $\langle 01.8\rangle^*$, $\langle 01.5\rangle^*$ can be present. At the beginning of electrodeposition, the layer orientations are strongly influenced by the nature of the substrate, as well as by

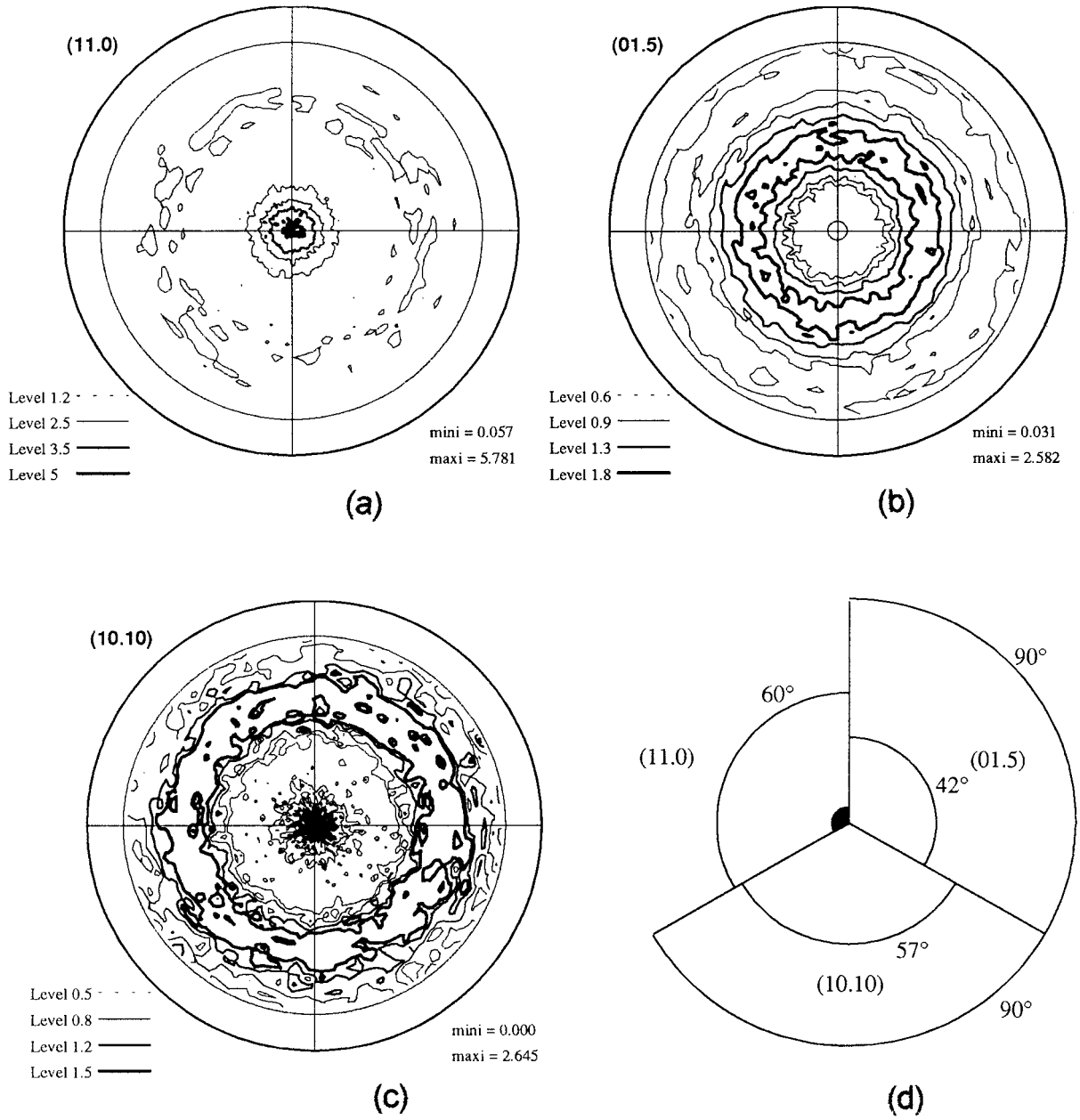

Fig. 5. Bi_2Te_3 sample of 20 μm thick, deposed on stainless steel. (a) Pole figure (11.0); (b) pole figure (01.5); (c) pole figure (10.10); (d); stereographic projections of $[1\,1\,0]^*$ fibre. The theoretical location of the $h\,k\,l$ rings of each pole figure is drawn on each third.

the conditions of electrodeposition. After some micrometres of growth, the layer has new fibre orientation $\langle 11.0\rangle^*$, which remains the same during the entire growth of the layer (Figure 9).

4. Bismuth telluride orientations explained

To explain the different orientations observed during the electrolytic deposition of thin layers of Bi_2Te_3, Hartman's theory, which predicts the equilibrium shape of crystals [2], was used since there is an analogy between the mechanism of crystal growth from a vapour or a solution and a layer growing by electrodeposition.

4.1. *Hartman's theory*

During the growth, a crystal is bounded by the faces of which edges are parallel to close packed directions (called dense directions by Hartman) $[u\,v\,w]$, in which there is an uninterrupted chain of strong bonds between atoms called 'periodic bond chain' or PBC The strong bonds are bonds in the first coordination sphere of an atom, ion or molecule. They are formed during the crystallization process. This PBC must have the composition of the crystal, no dipole momentum across the face and no other periods belonging to other chains.

According to Hartman's theory at the beginning of the growth, all the faces of the crystal can be present as shown in Figure 6(a) and (e). The crytallites have rather

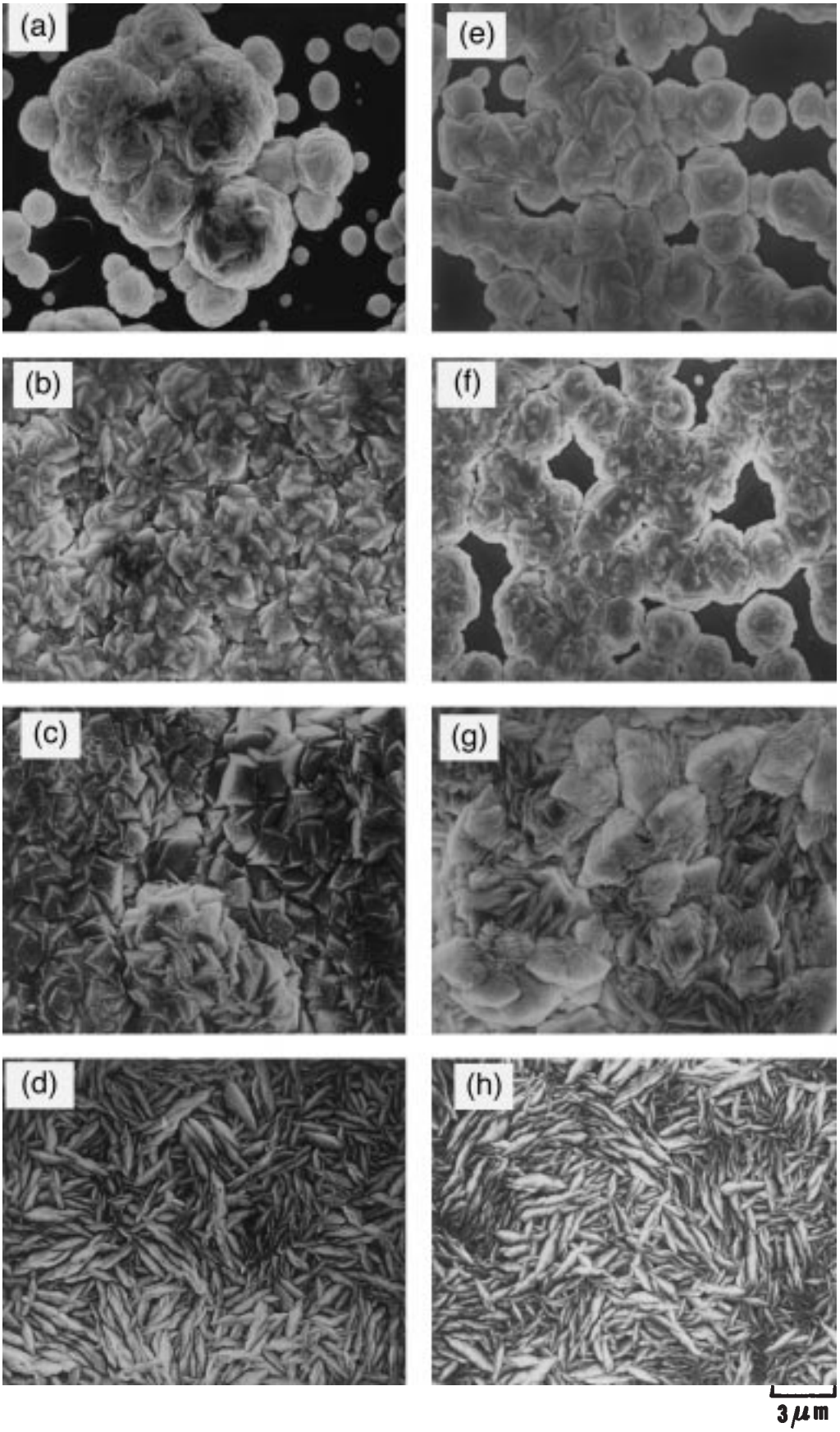

Fig. 6. Scanning electronic microscopy. Morphology of the layers according to their thickness 0.3 μm (a, e), 1 μm (b, f), 5 μm (c, g) and 20 μm (d, h). Electrodeposited on aluminium (a, b, c, d) and electrodeposited on stainless steel (e, f, g, h).

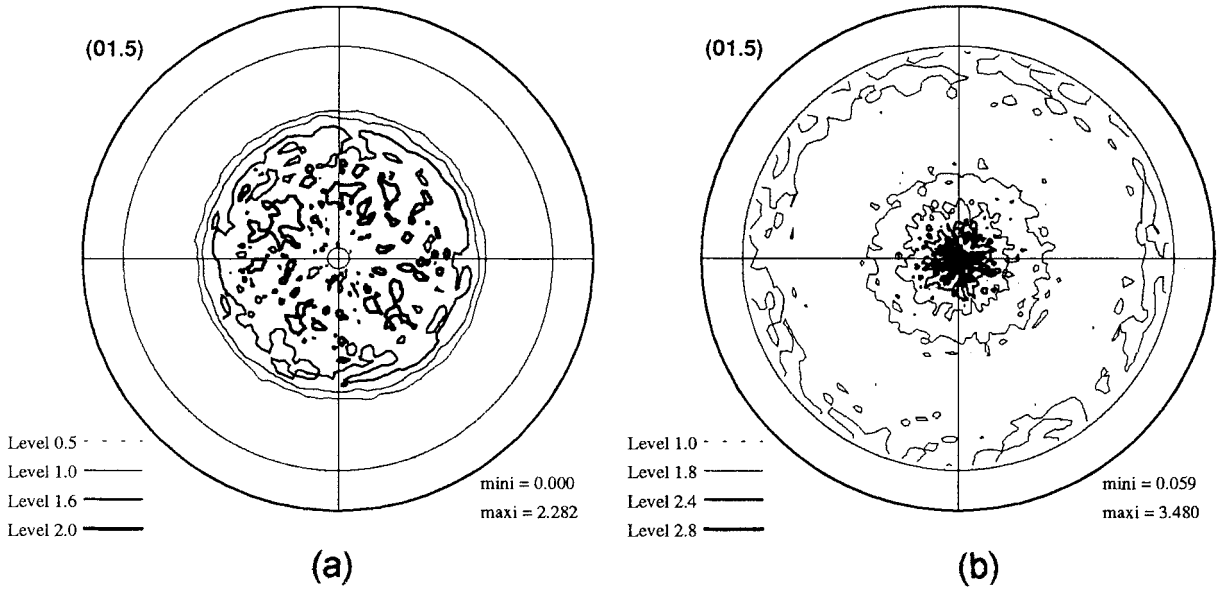

Fig. 7. Bi_2Te_3 sample of 5 μm thick deposited on (a) stainless steel and (b) aluminium.

a spherical shape, where many faces can be observed. These 'spheres' being distributed more or less randomly on the substrate, leads to an isotropic layer as assumed from the pole figure observation.

During growth (Figure 10), the K faces (with none PBC), initially disappear, then the S faces (with one PBC) disappear also. At the end the crystal reaches an equilibrium constituted by only F faces,which have at least two PBC. In Figure 6(d) and (h), the crystallites with a stick shape mainly show these faces; these are probably the (11.0) faces because the pole figure observation has shown that the (11.0) lattice planes are parallel to the substrate.

Figure 11(a) represents a grain of the layer during its growth, two faces and a unit of growth are shown. The intersection of the two faces is a dense row $[u\,v\,w]$. Along the direction $[u\,v\,w]$ (Figure 11(b)) the atoms are spaced periodically with a period λ and make the PBC $[u\,v\,w]$. The projection of such PBC in a plane perpendicular to $[u\,v\,w]$ are represented by closed polygons, making a two dimensional lattice, whose periodicity reflects the unit of growth having a thickness $d(h\,k\,l)$.

4.2. *Research of PBC*

4.2.1. *Strong bonds*

To determine strong bonds, we have calculated the distance between atoms of tellurium and bismuth (Figure 3). The bonds between first neighbours are the

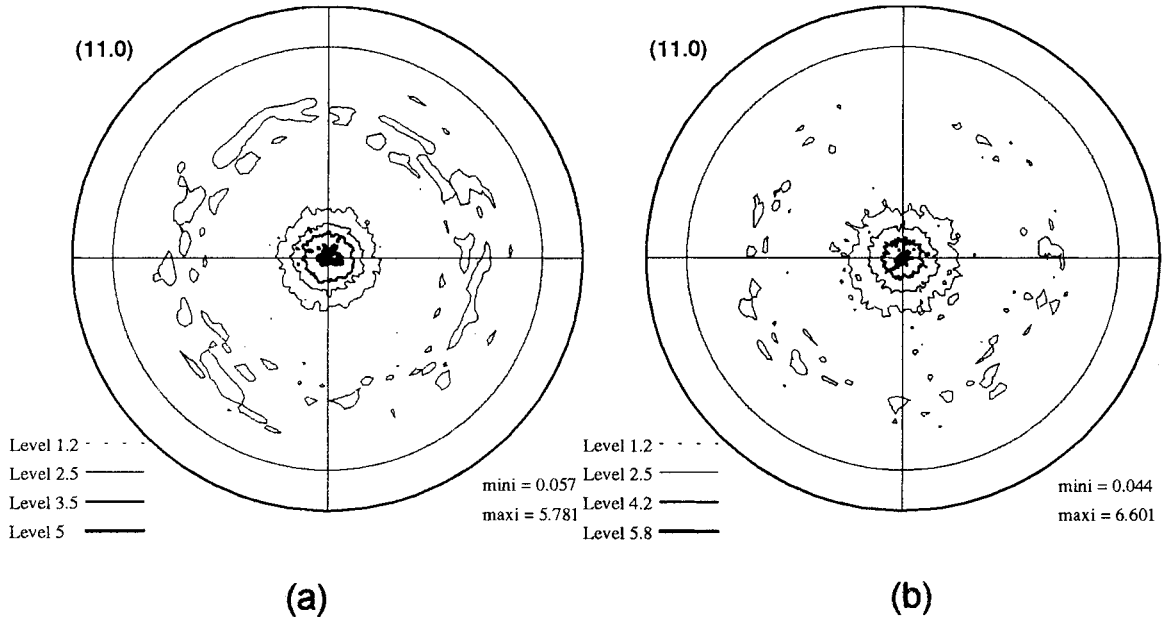

Fig. 8. Bi_2Te_3 sample of 20 μm thick, deposited on (a) stainless steel and (b) aluminium.

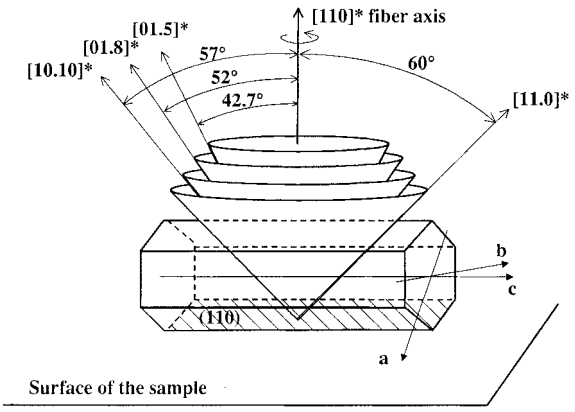

Fig. 9. Orientation of a grain having the $[1\,1\,0]^*$ fibre orientation. The hexagonal prism, represented in a given position, can have all the orientations keeping the lattice plane $(1\,1\,0)$ parallel to the surface. In this case the normal to other lattice planes describe cones which are represented by rings on the pole figures.

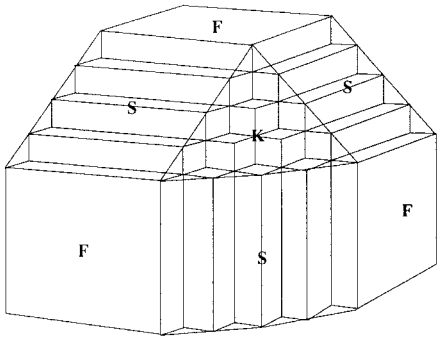

Fig. 10. Growth faces of a hypothetical crystal (Hartman).

'short bonds': $Te^{(1)}$–Bi = 3.22 Å and $T^{(2)}$–Bi = 3.042 Å and the bonds between second neighbours are the 'long bonds': $Te^{(1)}$–Bi = 5.412 Å and $T^{(2)}$–Bi = 5.021 Å.

4.2.2. *Close packed rows*

To proceed from a tellurium atom to the other equivalent tellurium atom on the row $[u\,v\,w]$ several paths consisting of strong bonds may exist . A path is a PBC in the direction $[u\,v\,w]$ if it fulfils the conditions defined by Hartman.

The most important rows to take into account are the most dense: $[0\,\bar{1}\,0]_H$, $[\bar{2}\,\bar{1}\,0]_H$, $[\bar{1}\,\bar{2}\,1]_H$, $[\bar{4}\,\bar{2}\,1]_H$, and $[\bar{1}\,\bar{5}\,1]_H$.

4.2.3. *Determination of the layer of growth*

As an example the projection of Bi_2Te_3 parallel to the direction $[0\,\bar{1}\,0]_H$ is shown in Figure 12. Different layers of growth $(10.1)_H$, $(01.5)_H$, $(003)_H$, $(10.8)_H$ are drawn. After all the projections of PBC parallel to all $[u\,v\,w]$ previously given, a complete evaluation of the layers of growth is presented in Table 1. Some layers have two or more PBC, and others only one PBC. So the layers of growth $(10.1)_H$ have two PBC in the direction $[\bar{1}\,\bar{2}\,1]_H$ and $[0\,\bar{1}\,0]_H$ while $(01.5)_H$ has only one PBC.

A comparison between Table 1 and the different fibres axes observed during the growth of the electroplated layer shows a good agreement between the S and F layers of growth and the fibre axis. Moreover, when the layer is thick enough, only the $[11.0]^*_H$ fibre axis is present and this corresponds to an F face.

For a given volume of crystallite, Gibbs and Curie defined its equilibrium shape as that possessing the minimal total energy:

$$\phi = \sum \gamma_i \times A_i$$

where γ_i is the specific surface energy of the crystallographic face i having an area A_i[15]. γ_i is also defined as the bounding energy of the unit of growth per unit area [16]. The more developed faces are those having the

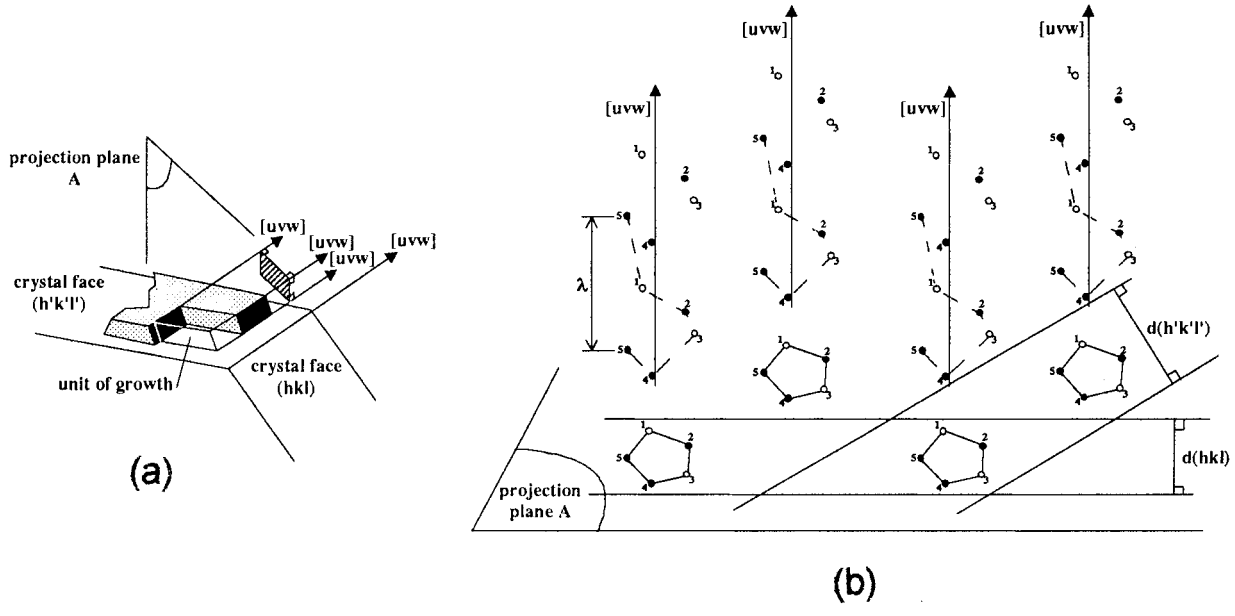

Fig. 11. Hartman principle. (a) Progress of a face during the crystal growth; (b) projection of the atomic structure along $[u\,v\,w]$ in a plane perpendicular to $[u\,v\,w]$.

Table 1. Apparition frequency of layers of growth ($h\ k\ l$) along the projection direction [$u\ v\ w$]

Projection direction or PBC	Layers of growth $(h\ k\ l)_H$ (H = hexagonal indexes)							
	$\{10.1\}_H$	$\{11.0\}_H$	$\{01.2\}_H$	$\{01.5\}_H$	$\{10.4\}_H$	$\{00.1\}_H$	$\{10.8\}_H$	$\{11.3\}_H$
$[\bar{1}\,\bar{2}\,1]_H$	*	*	*					
$[0\,\bar{1}\,0]_H$	*			*	*	*	*	
$[\bar{4}\,\bar{2}\,1]_H$		*	*		*			
$[\bar{2}\,\bar{1}\,0]_H$						*		
$[\bar{1}\,\bar{5}\,1]_H$					*			*

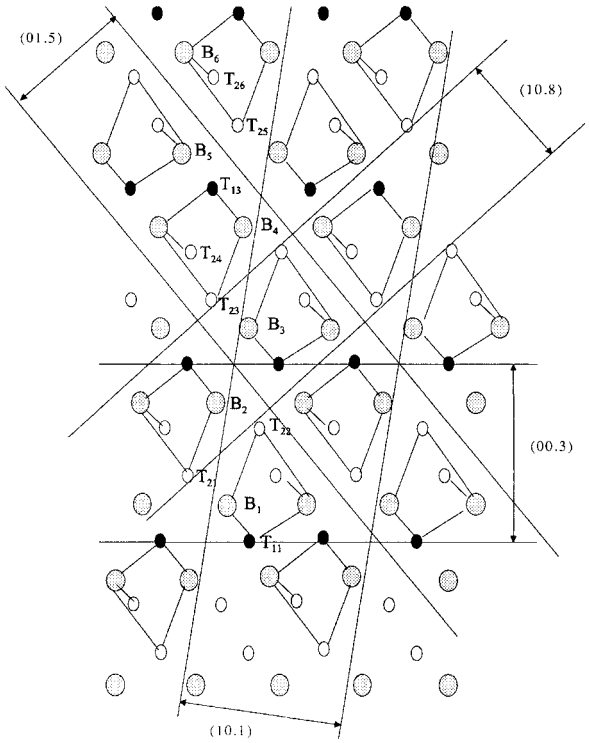

Fig. 12. Projection of the bismuth telluride structure parallel to $[0\,\bar{1}\,0]_H$ on the perpendicular plane. The layers of growth $(00.3)_H$, $(01.5)_H$, $(10.1)_H$ and $(01.8)_H$ are defined on this projection.

smaller γ_i. Growing rates of these faces, which would remain at the end of the growth, are smaller.

According to Hartman's theory the layer of growth occurs when strong bonds exist between PBCs of the unit of growth and the face. γ_i can be also defined as the number of bonds per unit area between these PBC. Different values of γ_i for the F faces suggest a range with an increasing order according to the probability of their stability: That is,

$$(11.0)_H > (01.2)_H > (10.4)_H > (10.1)_H > (00.1)_H$$

The face $(11.0)_H$ will be the most extended and grows parallel to the substrate.

The same kind of results [17, 18] are also observed for the copper layers. At the beginning of electrodeposition, the layers are randomly oriented, then [$h\ h\ l$], [1 1 1] and [1 0 0] fibre orientations appear (S and F faces). When the layer is sufficiently thick, only the [1 1 1] or [0 0 1] orientations remain, corresponding to units of growth which give F faces [4].

When the substrate influence becomes negligible, it seems that faces having the smaller surface energy grow parallel to the sample surface.

5. Conclusion

Electrodeposited layers of bismuth telluride $Bi_{2-x}Te_{3+x}$ have a fibre texture. The fibre axes depend on conditions of electrodeposition. The thickness of the layer is the most important parameter: when the layer is sufficiently thick ($e > 10\,\mu m$) the $[1\,1\,0]^*_H$ fibre axis remains, whatever the substrate.

At the beginning of the growth, the unit of growth defined by Hartman can be considered as nuclei which have several orientations depending on their number of PBC (K, S and F faces). As the thickness increases, only the growing layers with one or two PBCs can exist. When the layer reaches a sufficient thickness, only the $[1\,1\,0]^*_H$ orientation remains, corresponding to an equilibrium F face of the growth.

The geometrical aspect of the Hartman theory allows us to anticipate layer orientations during electrodeposition. A thermodynamic extension of the theory would further improve these results.

Acknowledgement

Authors thank Professor J.M. Lecuire, (CNRS – URA 158) of the University of Metz who provided the Bi_2Te_3 samples.

References

1. D.B. Knorr and D.P. Tracy, International Conferences on Texture of Material, ICOTOM 10 (1993) 1443–8.
2. I. Handreg and P. Klimanek, *Materi. Sci. Forum* **157–162** (1994) 1405–10.
3. H. Chaouni, PhD thesis, University of Metz (1995).
4. P. Hartman, 'Crystal Growth' (Elsevier, 1973), p.376.
5. P. Hartman, J. Cryst. Growth **63** (1983) 261–4.
6. J.H. Horst and R.M. Geertman, *Acta Cryst*. Section A vol A52 Supplement Pp C516 Iucr XVII Congress, Seattle (1996).
7. L.G. Schulz, *J Appl. Phys.* **20** (1949) 1030–33.
8. M.J. Bunge, 'Mathematische Methoder der Texturanalyse' (Academic- Verlag, Berlin, 1969).
9. J.J. Heizmann, C. Laruelle and A. Vadon, *J. Appl. Crystallogr*. **19** (1986) 467–72.
10. P. Magri, C. Boulanger and J.M. Lecuire, *J. Mater. Chem*. **6** (1996) 773–9.

11. J.P. Fleurial, PhD thesis à l'I. N.P.L., University of Nancy (1988).
12. H. Chaouni, P. Magri, J. Bessières, C. Boulanger and J.J Heizmann, *Mater. Sci. Forum* **157–162** (1994) 1371–77.
13. L. Kullmann, *Phys. Status Solidi B* (1984) 125–31.
14. J.R. Weise and L. Muldawer, *J. Phy. Chem Solids*. **15** (1960) 13–16.
15. S. Toschev, 'Crystal Growth' (Elsevier, 1973), p. 328.
16. P. Bennena, 'Crystal Growth' (Elsevier, 1973), p. 342.
17. H. Chaouni, J. Bessières and J.J. Heizmann, International Conferences in Texture of Material, ICOTOM 11 **2** (1996) 1118–25.
18. I. Handreg and P. Klimanek, International Conferences on Texture of Material, ICOTOM 10 (1993) 1405–10.